

ϕ_2/α

C.C.Wang

Department of Physics, National Taiwan University, No.1, Sec.4, Roosevelt Rd., Taipei, Taiwan, 106

We report the recent ϕ_2/α results from Belle with KEKB accelerator and Babar with PEP-II accelerator. The analysis of $B \rightarrow \pi\pi$, $B \rightarrow \rho\rho$ and $B \rightarrow \rho\pi$ are included in this report. These $b \rightarrow u\bar{u}d$ decay modes are related to the CKM angle ϕ_2/α and the method of ϕ_2/α extraction of corresponding decays are also included. After combining all the decay modes, the constraint of ϕ_2/α is $(100.2^{+15.0}_{-8.8})^\circ$.

1. Introduction

In the Standard Model (SM), CP violating effects in the B meson system can be parameterized in terms of three Cabibbo-Kobayashi-Maskawa (CKM) [1] phase angles ϕ_1 , ϕ_2 and ϕ_3 (which can be also written as β , α and γ , respectively). The angle ϕ_2/α can be extracted via the $b \rightarrow u\bar{u}d$. Approaches for ϕ_2/α extraction from the isospin analysis, $B \rightarrow \pi\pi$ and $B \rightarrow \rho\rho$, and the time-dependent Dalitz analysis, $B \rightarrow \rho\pi$ are reported in this document.

The experimental measurements are from B-factories, Belle detector with KEKB accelerator and Babar detector with PEP-II accelerator. These two detectors are general purpose detectors with energy-asymmetric e^+e^- accelerators. The Belle detector consists of a silicon vertex detector (SVD), a central drift chamber (CDC), an array of aerial threshold Čerenkov counters (ACC), time-of-flight scintillation counters (TOF), and an electromagnetic calorimeter (ECL) comprised of CsI(Tl) crystals located inside a superconducting solenoid coil that provides a 1.5 T magnetic field. An iron flux return located outside of the coil is instrumented to detect K_L^0 mesons and identify muons. The Babar detector contains silicon vertex tracker (SVT), drift chamber, electromagnetic calorimeter, ring-imaging Čerenkov detector (DIRC) and a 1.5 T solenoid superconducting magnet.

2. $B \rightarrow \pi\pi$

In the $B^0 \rightarrow \pi^+\pi^-$ decay, the time dependent rate is described by

$$\mathcal{P}^q(\Delta t) = \frac{e^{-|\Delta t|/\tau_{B^0}}}{4\tau_{B^0}} [1 + q \cdot \{\mathcal{S}\sin(\Delta m_d \Delta t) + \mathcal{A}\cos(\Delta m_d \Delta t)\}]. \quad (1)$$

The notation \mathcal{A} is used by Belle collaboration which is the same as $-\mathcal{C}$ used by Babar collaboration.

The $B^0 \rightarrow \pi^+\pi^-$ analysis uses 253 fb^{-1} data collected by Belle [2]. Signal candidates are reconstructed by opposite charged tracks which are identified as pions and the pion identification is based on the combined information from the ACC and the

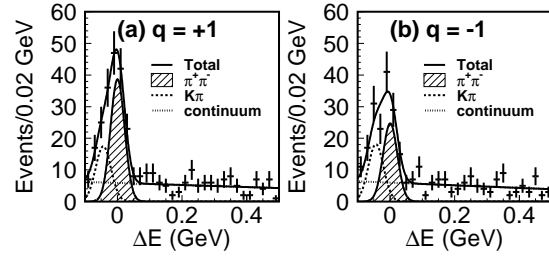


Figure 1: ΔE distributions in the M_{bc} signal region ($5.271 \text{ GeV}/c^2 < M_{bc} < 5.287 \text{ GeV}/c^2$) for $B^0 \rightarrow \pi^+\pi^-$ candidates with $\mathcal{LR} > 0.86$ for (a) $q = +1$ and (b) $q = -1$ from Belle.

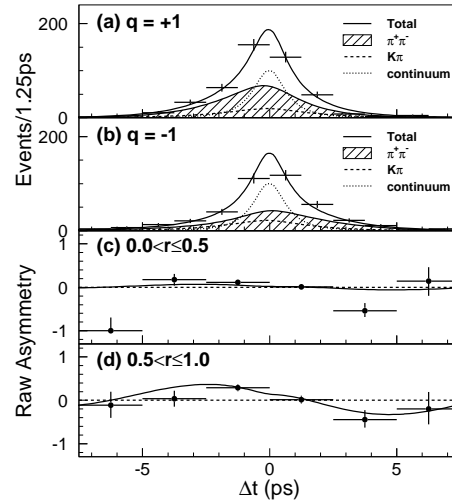


Figure 2: The Belle $B^0 \rightarrow \pi^+\pi^-$ Δt distributions for the candidates with $\mathcal{LR} > 0.86$ in the signal region ($5.271 \text{ GeV}/c^2 < M_{bc} < 5.287 \text{ GeV}/c^2$ and $|\Delta E| < 0.064 \text{ GeV}$). (a) $q = +1$ and (b) $q = -1$. Raw asymmetry, \mathcal{A}_{cp} , in each Δt bin with (c) $0 < r \leq 0.5$ and (d) $0.5 < r \leq 1.0$. The solid lines shows the result of the unbinned maximum likelihood fit.

CDC dE/dx measurements. B meson candidates are selected by using the energy difference $\Delta E \equiv E_B^* - E_{beam}^*$ and the beam-energy constrained mass $M_{bc} \equiv \sqrt{(E_{beam}^*)^2 - (p_B^*)^2}$, where E_{beam}^* is the CMS beam-energy, and E_B^* and p_B^* are the CMS energy and momentum of the B candidate, respectively. The flavor of accompanying B meson is identified from the inclusive properties of particles which are not used for

$B^0 \rightarrow \pi^+\pi^-$ reconstruction. To suppress the continuum background ($e^+e^- \rightarrow q\bar{q}$; $q=u,d,s,c$), the likelihood ratio (\mathcal{LR}) of the event topology based on signal MC and sideband data is used for continuum suppression. The likelihood ratio is optimized separately for each flavor tagging quality region. The tagging quality is monitored by variable r . After applying all above requirement and vertex reconstruction algorithm, 2820 signal candidates containing 666 ± 43 $\pi^+\pi^-$ signal events (1486 B^0 tags and 1334 \bar{B}^0 tags) are obtained. The CP violation parameters \mathcal{S} and \mathcal{A} are determined from the unbinned maximum likelihood fit to the proper-time difference Δt distribution. They obtained $\mathcal{S} = -0.67 \pm 0.16(\text{stat}) \pm 0.06(\text{syst})$ and $\mathcal{A} = +0.56 \pm 0.12(\text{stat}) \pm 0.06(\text{syst})$. The correlation between \mathcal{S} and \mathcal{A} is $+0.09$. Figure 1 and Figure 2 show the result from Belle.

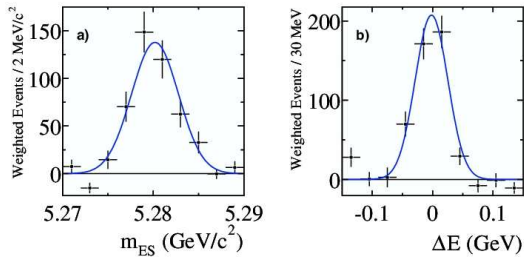


Figure 3: Babar's (a) m_{ES} and (b) ΔE distributions for $B^0 \rightarrow \pi^+\pi^-$. Solid curves represent the corresponding PDFs used in the fit.

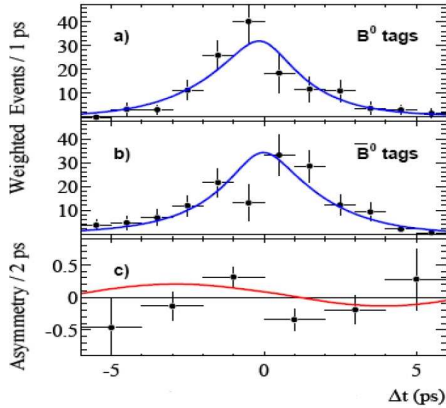


Figure 4: Babar's Δt distributions for $B^0 \rightarrow \pi^+\pi^-$. (c) raw asymmetry for signal events in each Δt bin.

The Babar's $B^0 \rightarrow \pi^+\pi^-$ analysis [3] is based on 211 fb^{-1} data. Signal candidates are reconstructed from opposite charged tracks with associated Čerenkov angles (θ_c). The particle identification is primarily accomplished by including θ_c in the maximum-likelihood fit. The kinematic variables ΔE and $M_{ES} = \sqrt{(s/2 + \mathbf{p}_i \cdot \mathbf{p}_B)^2 / \mathbf{E}_i^2 - \mathbf{p}_B^2}$ are used to identify the signal decays. Here \mathbf{p}_B is the B momentum and (E_i, \mathbf{p}_i) is the four-momentum of e^+e^-

initial state in lab frame. The background suppression is based on the angle of sphericity axes and Fisher discriminant \mathcal{F} formed from the momentum flow relative to $\pi^+\pi^-$ thrust axis. Unbinned extended maximum-likelihood fit is used to extract CP parameters and the likelihood function includes event yield, tagging efficiency, m_{ES} , ΔE , \mathcal{F} , θ_c^+ , θ_c^- and Δt . The fit yields $\mathcal{S} = -0.30 \pm 0.17(\text{stat}) \pm 0.03(\text{syst})$ and $\mathcal{C} = -0.09 \pm 0.15(\text{stat}) \pm 0.04(\text{syst})$ from 467 ± 33 $B^0 \rightarrow \pi^+\pi^-$ events. Figure 3 and Figure 4 show the result from Babar.

Using the model-independent isospin analysis [4, 5], the range of $[19^\circ, 71^\circ]$ for ϕ_2/α is excluded by Belle with 94.5% C.L. whereas $[29^\circ, 61^\circ]$ is excluded by Babar with 90% C.L.

3. $B \rightarrow \rho\rho$

The Babar's analysis of $B^0 \rightarrow \rho^0\rho^0$ [6] is performed with 211 fb^{-1} data. The reconstruction is made with four charged tracks and the particle identification is provided by the combining information from DIRC and SVT. The continuum suppression is performed based on the angle of thrust axis and neural network output variable \mathcal{E} . Unbinned maximum likelihood fit is used to extract the branching fraction by combining m_{ES} , ΔE , $\pi^+\pi^-$ invariant mass, ρ helicity angle and flavor tagging. From the fit, they obtain the upper limit of 1.1×10^{-6} at 90% C.L. The m_{ES} distribution is shown in Figure 5.

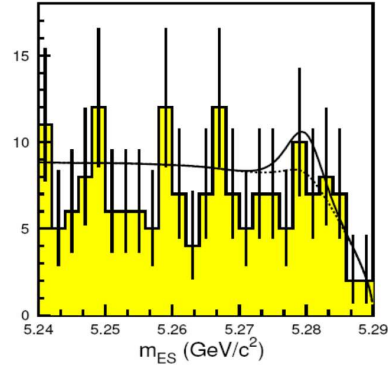


Figure 5: Projection of $B^0 \rightarrow \rho^0\rho^0$ m_{ES} distribution obtained at Babar.

The time dependent rate of $B^0 \rightarrow \rho^+\rho^-$ can be parametrized by the same form as Eq. 1.

The time-dependent CP analysis from Babar is performed with 211 fb^{-1} [7]. Comparing to $B \rightarrow \pi^+\pi^-$ analysis, the $B^0 \rightarrow \rho^+\rho^-$ need an angular analysis to extract the fraction for longitudinal component (f_L). An extended maximum-likelihood fit provides $f_L = 0.978 \pm 0.014(\text{stat})_{-0.029}^{+0.021}(\text{syst})$ and time-dependent CP parameters, $\mathcal{C}_L = -0.03 \pm 0.18(\text{stat}) \pm 0.09(\text{syst})$ and $\mathcal{S}_L = -0.33 \pm 0.24(\text{stat})_{-0.14}^{+0.08}(\text{syst})$. Figure 6 and

Figure 7 show the result of Babar's analysis. From the isospin analysis, Babar obtains ϕ_2/α between 79° and 123° with 90% C.L. which is based on the results of $B^0 \rightarrow \rho\rho$ mentioned above, the branching fraction of $B^0 \rightarrow \rho^+\rho^-$ [8, 9] and the results of $B^+ \rightarrow \rho^+\rho^0$ analysis [10, 11].

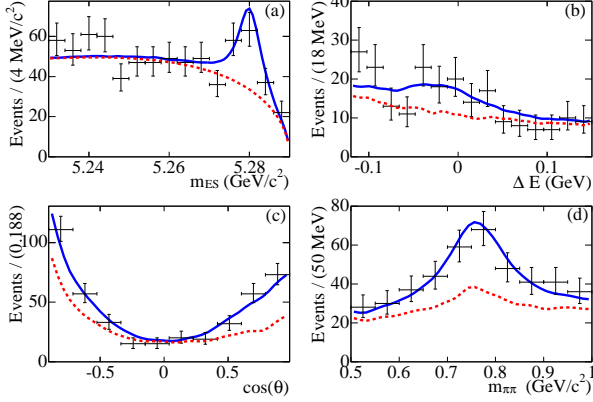


Figure 6: The distribution for the high purity events for variables (a) m_{ES} , (b) ΔE , (c) cosine of ρ helicity angle, and (d) $m_{\pi^+\pi^0}$. The dotted curves are the sum for all backgrounds and the solid lines are the total PDF.

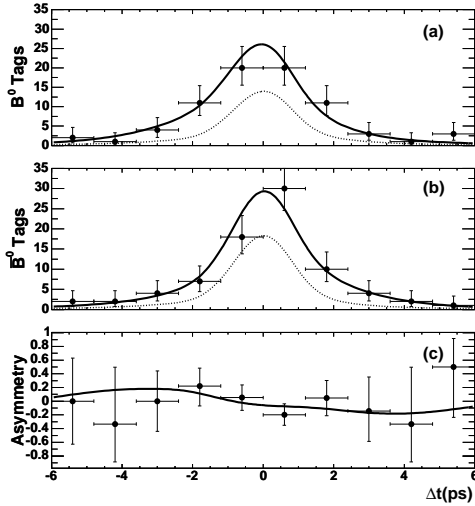


Figure 7: The Δt distribution for the signal enriched sample. (a) is B^0 tagged and (b) is \bar{B}^0 tagged events. (c) is the Δt raw asymmetry.

The time-dependent CP analysis from Belle is based on 253 fb^{-1} [12]. First, the longitudinal component fraction, $f_L = 0.941^{+0.034}_{-0.040}(\text{stat}) \pm 0.030(\text{syst})$, and time-dependent parameters, $\mathcal{A}_L = 0.00 \pm 0.30(\text{stat}) \pm 0.09(\text{syst})$ and $\mathcal{S}_L = 0.08 \pm 0.41(\text{stat}) \pm 0.09(\text{syst})$, are obtained. Figure 8, Figure 9 and Figure 10 show the result of Belle's analysis. Combining other related results [6, 8, 13], Belle obtain $59^\circ < \phi_2(\alpha) < 115^\circ$ with 90% C.L.

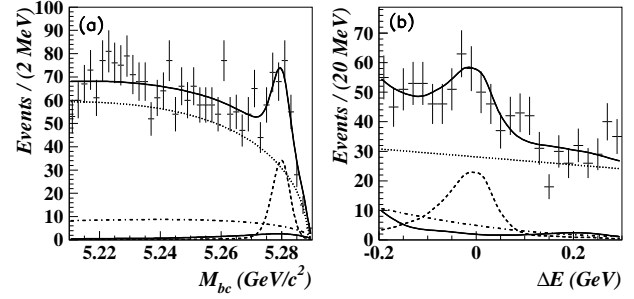


Figure 8: (a) M_{bc} projection in $-0.10\text{GeV} < \Delta E < 0.06\text{GeV}$ region. (b) ΔE projection in M_{bc} signal region. The dashed, dotted, dot-dashed, small solid and large solid curves show $\rho^+\rho^- + \rho\pi\pi$, $q\bar{q}$, $b \rightarrow c$, $b \rightarrow u$ and the total, respectively.

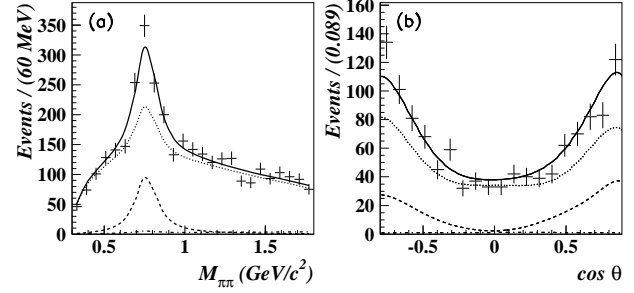


Figure 9: (a) $M_{\pi^+\pi^0}$ projection. (b) sum of two cosine helicity angle distribution. Both plots are inside $M_{bc} - \Delta E$ signal region and satisfy $0.62\text{GeV}/c^2 < M_{\pi^+\pi^0} < 0.92\text{GeV}/c^2$. The dashed, dot-dashed, dotted and solid curves represent $\rho^+\rho^-$, $\rho\pi\pi$, $q\bar{q} + (b \rightarrow c) + (b \rightarrow u)$ and the total, respectively.

4. $B \rightarrow \rho\pi$

Besides $B \rightarrow \pi\pi$ and $B \rightarrow \rho\rho$ decays, the quasi-two-body analysis for $B \rightarrow \rho\pi$ decay is another candidate for the ϕ_2/α extraction. Belle collaboration performed the time-dependent analysis on $B \rightarrow \rho^\pm\pi^\mp$ with 140 fb^{-1} and obtained time-dependent CP parameters, $C_{\rho\pi} = 0.25^{+0.16}_{-0.17}(\text{stat})^{+0.02}_{-0.06}(\text{syst})$, $S_{\rho\pi} = -0.28^{+0.23}_{-0.22}(\text{stat})^{+0.10}_{-0.08}(\text{syst})$, $\Delta C_{\rho\pi} = 0.38^{+0.17}_{-0.18}(\text{stat})^{+0.02}_{-0.04}(\text{syst})$ and $\Delta S_{\rho\pi} = -0.30^{+0.24}_{-0.23}(\text{stat}) \pm 0.09(\text{syst})$, flavor integrated charge asymmetry, $A_{CP}^{\rho\pi} = -0.16^{+0.09}_{-0.10}(\text{stat}) \pm 0.02(\text{syst})$, and direct CP violation parameters, $A_{+-} = -0.02^{+0.16}_{-0.15}(\text{stat})^{+0.05}_{-0.02}(\text{syst})$ and $A_{-+} = -0.53^{+0.29}_{-0.28}(\text{stat})^{+0.09}_{-0.04}(\text{syst})$ [14].

The branching fraction of $B^0 \rightarrow \rho^0\pi^0$ is obtained to be $3.12^{+0.88}_{-0.82}(\text{stat}) \pm 0.33(\text{syst})^{+0.50}_{-0.68}(\text{model}) \times 10^{-6}$, and the CP asymmetry, $A_{CP} = -0.53^{+0.67}_{-0.84}(\text{stat}) \pm^{+0.10}_{-0.15}(\text{syst})$, are obtained by Belle with 357 fb^{-1} data [15].

Besides the quasi-two-body analysis, Babar performs the time-dependent Dalitz analysis from $B \rightarrow \rho\pi$ with $\pi^+\pi^-\pi^0$ final states [16] with 192 fb^{-1} data. It is the first direct measurement of ϕ_2/α by assum-



Figure 10: The Δt distribution inside $M_{bc} - \Delta E$ signal region and satisfy $0.62\text{GeV}/C^2 < M_{\pi^+\pi^0} < 0.92\text{GeV}/C^2$. (a) and (b) are the B^0 tagged and \bar{B}^0 tagged events. (c) is raw asymmetry for the events satisfy $0.5 < r \leq 1.0$.

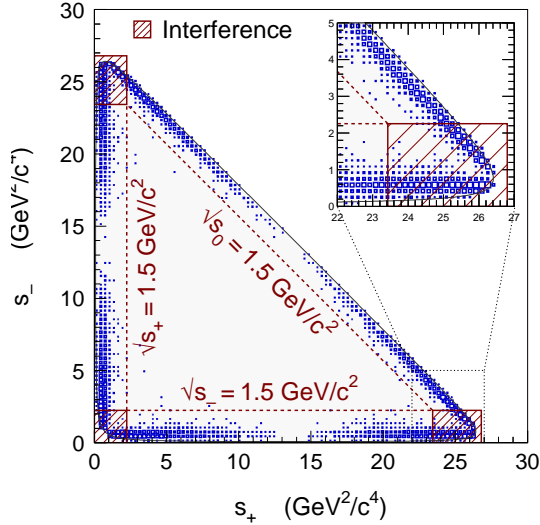


Figure 11: The Dalitz plot from $B^0 \rightarrow \pi^+\pi^-\pi^0$ Monte Carlo without detector simulation. $\rho^+\pi^-$, $\rho^-\pi^+$ and $\rho^0\pi^0$ are generated with equal amplitudes.

ing isospin symmetry. The decay amplitude can be expressed as

$$A_{3\pi} = f_+ A^+ + f_- A^- + f_0 A^0,$$

$$\bar{A}_{3\pi} = f_+ \bar{A}^+ + f_- \bar{A}^- + f_0 \bar{A}^0.$$

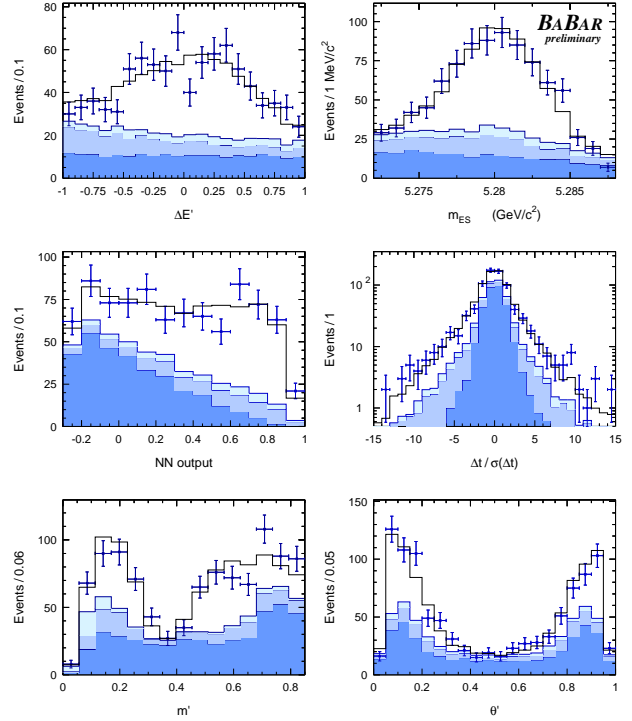


Figure 12: Distribution of $\Delta E'$, m_{ES} , neural network output, $\Delta t/\sigma(\Delta t)$, m' and θ' . The dark, medium and light shaded areas represent the contribution from continuum events, the sum of continuum events and the B background, and the mis-reconstructed signal events, respectively.

The f_+ , f_- and f_0 are functions of $\pi^\pm\pi^0$ invariant mass that incorporate the kinematic and dynamical properties of the B^0 decay into $\rho\pi$. The Dalitz plot distribution for Monte Carlo is shown in Figure 11. The time-dependent rate for B^0 and \bar{B}^0 tagged events are $|A_{3\pi}^+(\Delta t)|^2$ and $|A_{3\pi}^-(\Delta t)|^2$, respectively. The rates are given by

$$\begin{aligned} |A_{3\pi}^\pm(\Delta t)|^2 &= \frac{e^{-|\Delta t|/\tau_{B^0}}}{4\tau_{B^0}} [|A_{3\pi}|^2 + |\bar{A}_{3\pi}|^2 \\ &\mp (|A_{3\pi}|^2 - |\bar{A}_{3\pi}|^2) \cos(\Delta m_d \Delta t) \\ &\pm 2Im(\bar{A}_{3\pi} A_{3\pi}^*) \sin(\Delta m_d \Delta t)]. \end{aligned}$$

There are 27 coefficients for this time dependent Dalitz rate, 9 for exponential, 9 for cosine oscillation and 9 for sine oscillation terms. Since the $B \rightarrow \rho^0\pi^0$ branching ratio is very small, the $B \rightarrow \rho^0\pi^0$ related oscillation parameters are fixed to be zero and the effect is taken into account by systematics. Figure 12 shows the projection plots for $\Delta E'$, m_{ES} , neural network output for continuum background suppression, $\Delta t/\sigma(\Delta t)$, m' and θ' . The $\Delta E'$ is the transformed ΔE to deal with the π^0 energy dependence and the $\sigma(\Delta t)$ is the event-by-event error on Δt . The m' and θ' are transformed Dalitz vari-

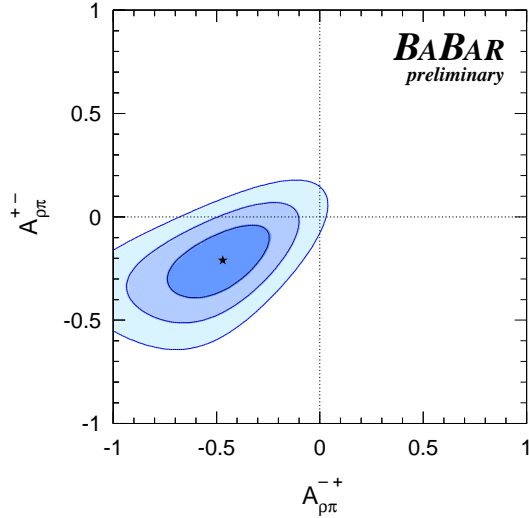


Figure 13: Confidence level contours for the direct CP violation. The shaded areas represent 1σ , 2σ and 3σ contours, respectively. The $A_{\rho\pi}^{+-}$ and $A_{\rho\pi}^{-+}$ here correspond to the Belle's A^{++} and A^{+-} , respectively.

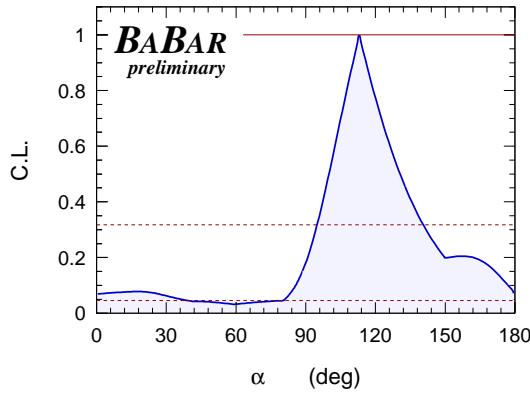


Figure 14: Confidence level functions for ϕ_2/α . The dashed horizontal lines corresponds to 1σ and 2σ C.L.

ables. The fit yields the direct CP violation values $A_{\rho\pi}^{+-} = -0.21 \pm 0.11(\text{stat}) \pm 0.04(\text{syst})$ and $A_{\rho\pi}^{-+} = -0.47_{-0.15}^{+0.14}(\text{stat}) \pm 0.04(\text{syst})$. Figure 13 shows the confidence level of direct CP violation. ϕ_2/α obtained from this analysis is $(113_{-17}^{+27}(\text{stat}) \pm 6(\text{syst}))^\circ$ and confidence level plot is shown in Figure 14.

5. Summary

From the $B \rightarrow \pi\pi$, $B \rightarrow \rho\rho$ and $B \rightarrow \rho\pi$ analysis, Belle and Babar obtained ϕ_2/α for each decay separately. The CKM Fitter Group performs a global fit by properly averaging all the results and get $\phi_2/\alpha = (100.2_{-8.8}^{+15.0})^\circ$ [17]. Figure 15 shows the result of this global fit for ϕ_2/α .

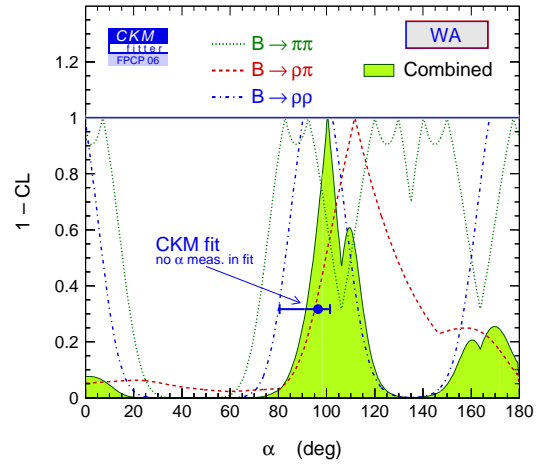


Figure 15: The combined ϕ_2/α constraint from CKM fit-ter Group.

References

- [1] M. Kobayashi and T. Maskawa, *Progr. Theor. Phys.* **49**, 652 (1973).
- [2] Belle Collaboration, K. Abe *et al.*, *Phys. Rev. Lett.* **95**, 101801 (2005).
- [3] BaBar Collaboration, B. Aubert *et al.*, *Phys. Rev. Lett.* **95**, 151803 (2005).
- [4] M. Granau and D. London, *Phys. Rev. Lett.* **65**, 3381 (1990).
- [5] J. Charles *et al.*, *Eur. Phys. J. C* **41**, 1 (2005).
- [6] BaBar Collaboration, B. Aubert *et al.*, *Phys. Rev. Lett.* **94**, 131801 (2005).
- [7] BaBar Collaboration, B. Aubert *et al.*, *Phys. Rev. Lett.* **95**, 041805 (2005).
- [8] BaBar Collaboration, B. Aubert *et al.*, *Phys. Rev. Lett.* **93**, 231801 (2004).
- [9] BaBar Collaboration, B. Aubert *et al.*, *Phys. Rev. D* **69**, 031102 (2004).
- [10] BaBar Collaboration, B. Aubert *et al.*, *Phys. Rev. Lett.* **91**, 171802 (2003).
- [11] Belle Collaboration, J. Zhang *et al.*, *Phys. Rev. Lett.* **91**, 221801 (2003).
- [12] Belle Collaboration, A. Samov *et al.*, hep-ex/0601024.
- [13] PDG, S. Eidelman *et al.*, *Phys. Lett. B* **592**, 1 (2004).
- [14] Belle Collaboration, C.C. Wang *et al.*, *Phys. Rev. Lett.* **94**, 121801 (2005).
- [15] Belle Collaboration, J. Dragic *et al.*, hep-ex/0508007.
- [16] BaBar Collaboration, B. Aubert *et al.*, hep-ex/0408099.
- [17] http://www.slac.stanford.edu/xorg/ckmfitter/ckm_results_fpcp2006.html